ROYAL INSTITUTE
OF TECHNOLOGY

Numerical studies on receptivity and control of a three-dimensional boundary layer

Solmaz Akbaripour

Thesis submitted to The Royal Institute of Technology
for the Master's degree

Supervisors:
Ardeshir Hanifi , David Tempelmann

February 6, 2012

Abstract

Receptivity in three-dimensional boundary layer flow to localized roughness elements over a flat plate is studied by means of direct numerical simulations (DNS). The surface roughness is modeled by applying nonhomogeneous boundary conditions along the wall as well as considering as a surface deformation by inserting the bump shape into the numerical mesh. Under the assumption of the small amplitudes of the roughness, although different disturbances amplitudes are observed in the vicinity of the bump for the meshed and modeled case, the boundary layer response downstream of the roughness is independent of the way of the bump implementation. Different roughness heights are considered in order to compare the boundary layer response of two approaches. Also, the boundary layer is excited by random distributed surface roughness and the receptivity results are studied. Moreover, a simple model for natural roughness excites steady multi wavenumber crossflow instabilities. A localised surface roughness i.e. *control roughness* is applied to stabilise the latter. The *control* mode which is subcritical with respect to transition affects the most steady unstable mode. Suppression of the most dangerous mode is observed through nonlinear interactions with the *control* mode.

Aknowledments

I would like to acknowledge both my supervisors, Prof. Ardeshir Hanifi and Dr. David Tempelmann for their kind supports during my master thesis. Thanks Ardeshir for the nice disscussions and providing me with your deep knowledge. Thanks David for your guidance and patiance with me during all steps of my master thesis.

I am grateful to my teacher Prof. Luca Brandt for his valuable advices during my master studies. My colleagues and friends at KTH are also aknowledged for nice discussions and friendly environment.

I would also like to thank my mom & dad, and Saviz & Hamedeh. Thank you for your constant care and encouragements to gain my goals. Finally, special thanks to my boyfriend Mohammad, for his love and endless support.

Contents

Chapter 1

Introduction

The concept of transition from laminar to turbulent flow is interesting due to its practical importance in engineering applications, since transition affects essential aerodynamic quantities such as drag or heat transfer.[8] The transition process is started by receptivity which refers to the penetration of external disturbances such as surface roughness, free-stream disturbances, etc. into the boundary layer and supplying conditions for the instability initiation. The process is followed by linear and nonlinear disturbances growth and finally results in the break-down to turbulent flow.

1.1 Three dimensional boundary layer

A boundary layer is generated because of a competition between frictional and inertial forces within a flow. Three-dimensional boundary layers appears on swept wings, rotating discs, cones, spheres, etc. Falkner-Skan-Cooke (FSC) boundary layers which represent a similarity solution of the boundary-layer equation give a good approximation of the flow over the swept wings [4]. This configuration includes most of the characteristics of the swept-wing boundary-layer flow such as the chordwise pressure gradient and the sweep angle.

A velocity component perpendicular to the inviscid streamline, i.e. the crossflow, appears due to an imbalance between the sweep angle and chordwise pressure gradient inside the boundary layer [5]. A curved streamline is formed due to the freestream acceleration and the mean flow is elongated in the free-stream direction rather than the chord- and spanwise directions. The external streamline and the FSC velocity profile are shown in figure 1.1. The occurring inflection point in the three-dimensional boundary layer velocity profiles leads to an inviscid inflectional instability. In order to understand the fundamental instability mechanisms which lead to transition to turbulence in swept-wing flows, studying three-dimensional boundary layers is motivated.

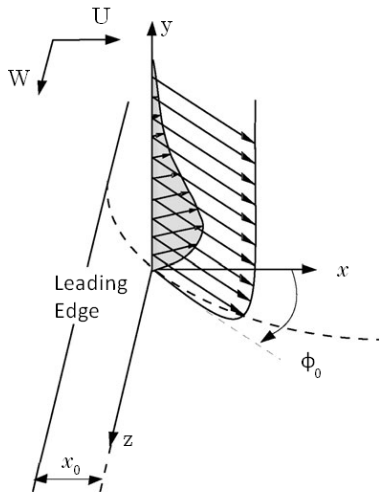

Figure 1.1: The streamwise and the crossflow velocity profiles for Falkner-Scan-Cooke boundary-layer [1].

The presence of the inflectional point in such a velocity profile results in both steady and travelling unstable waves, the so called crossflow vortices. These are almost aligned with the external streamlines. Although both stationary and travelling waves exist in a typical swept wing flow, transition usually occurs due to one of these two types of waves. Reibert and Saric (1997) have shown that the stationary crossflow modes dominate for low levels of the turbulence environment while according to Deyhle and Bippes (1996) and Bippes (1997) travelling waves dominate in a high-turbulence environment [3][12]. Here, we focus on stationary crossflow waves.

1.2 Receptivity

Receptivity analysis implies the part of the transition that describes the response of the boundary layer to external perturbations. If the external perturbations have the ability to feed the boundary layer eigenmodes with energy and result in modal and non-modal instabilities, one can say that the boundary layer is receptive to those disturbances [1]. External perturbations can be introduced into the boundary layer through a direct or an indirect mechanism. Receptivity

of the boundary layer flows to surface roughness and free-stream vortices are direct mechanism. On the other hand, the interaction of the acoustic waves with the roughness generates instability waves which provide an indirect instability mechanism.

The term receptivity was introduced by Morkovin (1968) for the first time, however Gaster dedicated a theoretical paper to this problem even earlier [7]. Our understanding of the receptivity process are largely based on asymptotic theories as pointed out by Goldstein (1983,1985) [9]. The earliest of these have been performed by Goldstein(1983, 1985) and Ruban (1985) who considered the receptivity at the first neutral point of Tollmien-Schlichting (TS) instability in Blasius flow [1].

1.3 Experimental studies on receptivity

Bippes did several experiments on receptivity and transition of three-dimensional boundary layers. The results show that stationary crossflow disturbances dominate transition in a low-turbulence environment while at high disturbance levels, the transition process is dominated by travelling crossflow waves. Steady crossflow waves are more practical due to representing a good deception in flight conditions compared to the travelling waves [19] [20].

The non-linear saturation of the stationary crossflow waves on a swept wing within a low-disturbance environment was investigated by Reibert *et al.* In their experiment, the roughness elements were applied in order to control the initial conditions as a result of applying surface irregularities near the leading edge. The results reveal that forcing the most unstable mode according to linear theory leads to nonlinear amplitude saturation of the disturbances well before transition. These data show failure of the stability linear theory to capture transition details for crossflow dominated boundary-layers. Also, the effect of surface roughness height has been investigated. The authors identified that although the initial disturbances amplitude increases by the increasing roughness height, saturation amplitude is almost independent of the bump height [3].

Saric *et al.* continued the experiments done by Reibert *et al.* (1996). They applied periodic array of roughness elements at the leading edge in order to force the steady crossflow disturbances. The roughness elements are arranged in a way that the spacing between the bumps is less than the wavelength of the most unstable mode. This approach is termed sub-critical roughness spacing. The disturbances excited are sub-critical with respect to transition. The results show suppression in disturbances amplitude for the linearly most unstable mode and a transition delay compared to the enforced. It was concluded that localising surface roughness can be used in order to control transition process on swept wings [17].

Radeztsky *et al.* observed that surface roughness plays the most important role in generating crossflow disturbances. The authors found that the transition location is quite sensitive to the roughness height even for quite low Re_k. Furthermore, the results show that there is a critical diameter below which the roughness has no influence on transition. Radeztsky *et al.* also investigated the natural surface roughness influence on the transition location. They identified that the transition Reynolds number increases while the roughness elements heights are decreased [14].

Gaponenko *et al.* studied the receptivity of a three-dimensional boundary layer to localized surface vibrations and roughness over a swept wing both theoretically and experimentally. Their results have shown that the receptivity coefficient is independent of the specific shape of the surface non-uniformities. Moreover, the vibration and roughness receptivity coefficients obtained through experiments are nearly independent of the disturbance frequency, and weakly dependent on the spanwise wavenumber [10]. Saric *et al.* reviewed the important findings of the 1990s on stability and transition in three dimensional boundary layer flows. The authors focused on the crossflow instability which results in transition on swept wings and rotating disks. They concluded that by studying the basic physics and applying the artificial roughness at the leading edge, controlling the crossflow instability and delaying transition on swept wings in flight are possible [12].

1.4 Finite Reynolds number theory (FRNT) and direct numerical studies (DNS) studies on receptivity

Zavol'skii *et al.* (1983) developed a method called finite Reynolds number theory (FRNT) for receptivity analysis which is valid at high Reynolds numbers. FRNT can be applied downstream and upstream of the first neutral point of the instability. This theory is based on one dimensional parallel flow and linear stability theory assumptions. According to this theory, the external disturbances such as surface roughness are modeled by non-homogeneous boundary conditions and the ones like acoustic waves are considered as additional forcing terms [1].

Fedorov (1988) has done the first theoretical studies of the effect of localized surface roughness on the excitation of the swept-wing cross-flow instability mode by means of FRNT [10]. Later, Crouch (1993) and Choudhari (1994) considered receptivity of Falkner-Skan-Cooke boundary layer due to surface roughness and acoustic free-stream perturbations. In the case of small amplitude roughness elements, they investigated linear receptivity. The latter excites steady crossflow instability while travelling crossflow modes are generated by imposing weak acoustic free-stream waves which are scattered on the surface roughness. The

authors found that although the receptivity coefficient which relates the initial instability amplitude to the amplitude of the perturbation source is higher in the unsteady receptivity mechanism, the steady case shows larger initial disturbances amplitude [1].

The receptivity to a spanwise-periodic, chordwise-localized surface roughness near a swept leading edge in a three-dimensional boundary layer flow has been considered by Collis and Lele. They obtained the results from Linearized Navier-Stokes (LNS) solutions and FRNT predictions. They found that the existence of the surface curvature enhances the receptivity efficiency over the entire unstable region and its effect is most significant near the lower branch of the neutral curve. On the other hand, the non-parallel effects attenuate the initial amplitude of the crossflow instability wave near the leading edge, downstream of the surface roughness.[11] Also, Bertolotti investigated the effect of mean-flow nonparallelism on receptivity to localized surface roughness for two flows, the swept-Hiemenz flow and the swept flat plate boundary layer studied by Bippes and colleagues (1996). He concluded that the receptivity coefficient decreases when nonparallel effect is taken into account which is in agreement with previous DNS results. Moreover, the results showed good agreement with the observed experimental findings [13].

Wassermann and Kloker applied spatial direct numerical simulations to study the crossflow-vortex-induced laminar breakdown in a decreasingly accelerated three-dimensional boundary layer over a flat plate. The authors found that the onset of secondary instability is strongly dependent on the maximal localized mean flow deceleration caused by vortices. They used upstream flow deformation (UFD) technique in order to nonlinearly suppress the naturally most unstable mode, i.e. the target mode, by the excited crossflow vortex-mode with the wavelength 2/3 of the target mode wavelength. They found that the suppression of the target mode by UFD is mainly caused by the two-dimensional meanflow distortion which is nonlinearly generated by the UFD vortices [6].

Laminar flow control with discrete Roughness Elements (DREs) based over a subsonic/transonic aircraft has been studied by Choudhari *et al.*. The non-linear evolution of the steady crossflow modes by means of using the parabolized stability equations (PSE) shows that an increase in the amplitude of the control mode results in reduction of the target mode amplitude. The corresponding reduction in the mode amplitude is followed by reduced linear growth rates of the secondary instabilities. Also, the authors noticed that the possibility of overcontrol at higher initial target mode amplitudes should be taken into account [18].

Recently, receptivity of FSC boundary layer flows to surface roughness over a flat plate has been investigated by Schrader *et al.* by using Direct Numerical Simulation (DNS). Receptivity of different roughness shapes and heights were studied by considering inhomogeneous boundary conditions. The authors con-

cluded that the receptivity coefficient is independent of the roughness shape as long as the chordwise extension of the roughness is smaller than the wavelength of the unstable mode. Also, it was shown that for roughness elements with a height of about 5% beyond the displacement thickness, receptivity is affected by nonlinearity which leads to a gradual decrease of the efficiency coefficient as the roughness height is increased [1].

1.5 Objectives

The objective of this thesis is to investigate the boundary-layer receptivity to surface roughness with different amplitudes and shapes in three dimensional boundary layers over a swept flat plate. As mentioned earlier, Schrader *et. al* (2009) used non-homogeneous boundary conditions for surface roughness modelling. Here, we reproduce some of the results obtained by Schrader *et al.* (2009) but use both modeled and meshed surface roughness and compare the results. Moreover, two sets of roughness elements are applied as control mechanisms to suppress the most amplified mode which is excited by surface irregularities near the leading edge.

Chapter 2

Flow configuration and numerical approach

2.1 Base flow

The flow over an infinite swept flat plate exposed to a pressure gradient is considered. The mean flow is obtained by solving the three-dimensional time-dependent incompressible Navier-Stokes equations with FSC velocity profiles prescribed as the inflow boundary conditions obtained through the similarity solutions of the boundary layer. This kind of boundary-layer flow is chosen since most of the main features of the swept wing flow such as the chordwise pressure gradient, the streamline curvature and the crossflow are comprised in FSC boundary layer. The relations presented in the following corresponds to the case studied by Schrader *et al.* (2009b). The chord- and spanwise velocities at the edge of the boundary layer are respectively defined as

$$U_e(x) \equiv \frac{U_e^*(x^*)}{U_{ref}} = \left(\frac{x^* + x_0^*}{x_0^*}\right)^m, \tag{2.1}$$

$$W_e \equiv \frac{W_e^*(x^*)}{U_{ref}} = tan\phi_0 = const. \tag{2.2}$$

with ϕ_0, the sweep angle at the reference position ${x_0}^*$ and $m = \beta_H/(2-\beta_H)$ a measure of the flow acceleration or deceleration. Here, U_{ref} is the edge chordwise velocity at ${x_0}^*$ and β_H is the Hartree parameter which specifies the mean pressure gradient. The parameters m, β_H, x_0 and ϕ_0 are chosen equal to 0.2, 0.333, 167 and 45°, respectively (Schrader *et al.* (2009b)).

Due to independency of FSC boundary-layer flows of the spanwise direction, the boundary-layer solution is governed by the two-dimensional equations. The similarity solutions for the free-stream velocity distribution in (1) and (2) are

obtained by transforming independent variables i.e. the chordwise and normal coordinates x^* and y^*, into one single similarity variable η,

$$\eta = \sqrt{\frac{m+1}{2}\frac{U_e^*(x^*)}{\nu^* x^*}}y^*. \tag{2.3}$$

so the relations for the chordwise and wall-normal mean velocities U^* and V^* can be re-arranged as functions of η and the chord- and spanwise mean velocities U^* and W^* can be introduced as

$$U^* = U_e^* f'(\eta), \tag{2.4a}$$
$$W^* = W_e^* g(\eta). \tag{2.4b}$$

By doing some algebra, the boundary-layer equations can be written in the form of a nonlinear ordinary differential equation for the functions $f(\eta)$ and $g(\eta)$

$$f''' + ff'' + \beta_H(1 - f'^2) \;=\; 0, \tag{2.5}$$
$$g'' + fg' = 0, \tag{2.6}$$

which are solved subject to the boundary conditions

$$\eta = 0 \;:\quad f = f' = g = 0, \tag{2.7a}$$
$$\eta \to \infty :\quad f \to 1,\; g \to 1. \tag{2.7b}$$

As a consequence, the self-similar solution for the chordwise and spanwise velocities U^* and W^* are obtained from $f'(\eta)$ and $g(\eta)$.

The variables are dimensionless here. Lengths are non-dimensionalized by the chordwise boundary-layer thickness δ_0^* at the reference location x_0^* and velocities by the chordwise boundary layer edge velocity U_e^* at the same position. The inflow Reynolds number which can be defined as

$$Re_{\delta_0{}^*} = \frac{U_{ref}{\delta_0}^*}{\nu^*}$$

is set to 220 for the present results. Accordingly, the local Reynolds number is obtained with respect to the local boundary layer edge velocity $U_e^*(x)$ and displacement thickness $\delta^*(x)$. The local displacement thickness δ^* and Reynolds number Re_{δ^*} are shown in figure 2.1.

2.2 Disturbance generation by surface roughness

In the following the receptivity of the steady crossflow modes to localized surface roughness is investigated. Chordwise localized, spanwise periodic roughness elements with different heights and spanwise wavenumbers are considered. This

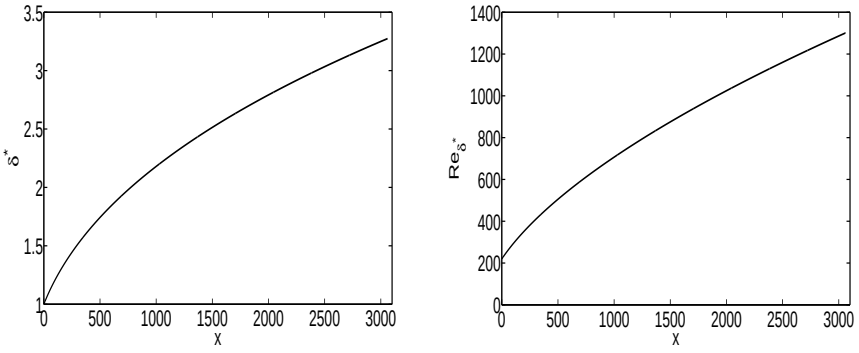

(a) (b)

Figure 2.1: (a) Chordwise boundary-layer displacement thickness and (b) Reynolds number as functions of the chordwise coordinate.

section reports how these roughness elements are modeled and implemented in the simulation code. Moreover, randomly distributed and a model for natural surface roughness is implemented and the corresponding boundary layer receptivities are investigated.

2.2.1 Chordwise localized, spanwise periodic bump

In the following, the surface roughness shape defined by Schrader *et. al* is considered. The roughness shape in the chordwise direction $h_x(x)$ is

$$h_x(x) = \left[S\left(\frac{x - h_{start}}{h_{rise}} \right) - S\left(\frac{x - h_{end}}{h_{fall}} + 1 \right) \right], \tag{2.8}$$

where the parameters h_{start} and h_{end} are the start and end positions of the roughness element, hence $h_x \neq 0$ between these two values. h_{rise} and h_{fall} indicate the extension of the rising and falling flanks of the smooth step function S

$$S(\xi) = \begin{cases} 0, & \xi \leq 0, \\ 1/(1 + \exp^{(1/(\xi-1)+1/\xi)}), & 0 < \xi < 1, . \\ 1, & \xi \geq 1. \end{cases} \tag{2.9}$$

Here, $h_{start} = 4.6$, $h_{end} = 32.2$ and $h_{rise} = h_{fall} = 11.5$. The chordwise localized, spanwise periodic surface roughness shape can be defined as

$$h(x, z) = \varepsilon_h h_x(x) sin(\beta_R z), \tag{2.10}$$

where ε_h is the maximum amplitude of the bump which is chosen as 0.021,

here. $\beta_R = 2\pi/L_z$ is the roughness element spanwise wavenumber and equal to 0.19. Consequently, the spanwise length scale of the surface roughness and the spanwise width of computational domain L_z are identical. The surface bump shape is shown in figure 2.2.

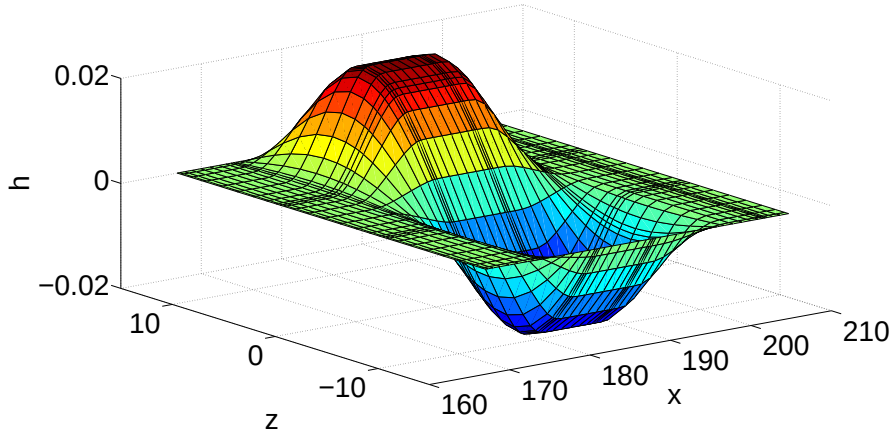

Figure 2.2: Roughness element shape in physical space.

Two approaches of modelling the roughness are considered i.e. meshed and modelled surface bumps. For the meshed case, the roughness element is considered as a surface deformation by including the bump into the numerical mesh. As a result, the wall includes the plate containing the disturbed surface, i.e. meshed roughness element.

For the modeled case, the surface roughness is not meshed but is modeled by applying non-homogeneous boundary conditions along the plate. These kind of boundary conditions are obtained by projection of the no-slip boundary conditions along the bump contour $h(x,z)$ on to the undisturbed wall $y = 0$ through a Taylor series expansion,

$$\begin{pmatrix} u \\ v \\ w \end{pmatrix}_0 = \begin{cases} \begin{pmatrix} -h(x,z)(\frac{\partial U}{\partial y} + \frac{1}{2}h(x,z)\frac{\partial^2 U}{\partial y^2}) \\ 0 \\ -h(x,z)(\frac{\partial W}{\partial y} + \frac{1}{2}h(x,z)\frac{\partial^2 W}{\partial y^2}) \end{pmatrix}_0, & h_{start} \le x \le h_{end}, \\ 0, & \text{elsewhere.} \end{cases} \tag{2.11}$$

Here, u, v and w are the chordwise, normal, and spanwise disturbance velocities, respectively. Taylor series expansion is truncated at either first or second order.

This allows to evaluate the order of accuracy of the assumption which has been made.

It should be mentioned that since inserting the surface roughness into the mesh gives more realistic results, all the receptivity results obtained by imposing inhomogeneous boundary conditions to model the surface bump are compared to the corresponding meshed ones. Furthermore, different roughness heights with the amplitudes equal to the original bump height multiplied by the factors 2, 5, 10, 14, 17, and 26 are taken into account. The boundary layer receptivity results regards to different bump amplitudes for both model approaches are studied and compared.

2.2.2 Receptivity coefficient of stationary modes in the presence of a single-wavenumber roughness element

Surface roughness is efficient if the roughness contour contains the wavenumber of the instability [15][16]. Receptivity is quantified in terms of the receptivity coefficient C_R which indicates the efficiency of the external forces to excite the least stable eigenmode of the boundary layer, here the surface roughness generates the steady crossflow mode. The receptivity coefficient C_R is a function of β_R, ω, m, and ϕ_0 where β_R is the spanwise wavenumber of the roughness element,

$$C_R = \frac{A_R}{\varepsilon_h H(\alpha_{CF})} \tag{2.12}$$

Here, A_R denotes so called receptivity amplitude, *i.e.* the equivalent amplitude that a clean crossflow mode should have in order to attain the same amplitude as the response at the position of the roughness element. H_R is the roughness shape h in Fourier space and α_{CF} is the chordwise wavenumber of the excited steady crossflow instability defined at the roughness position x_R. Various surface bumps are considered, differing in their heights as well as their spanwise wave number β_R.

2.2.3 Random distributed surface roughness

Natural surface roughness is modeled by a random distribution with an average height $8.5.10^{-4}$ over the whole plate by considering inhomogeneous boundary conditions according to (2.11). The roughness shape can be seen in figure 2.3. The box width L_z is 62.8 and consequently the fundamental wavenumber is obtained by $\beta_0 = 2\pi/L_z$. These surface irregularities enforce steady boundary-layer disturbances with different spanwise wavenumbers (β_R).

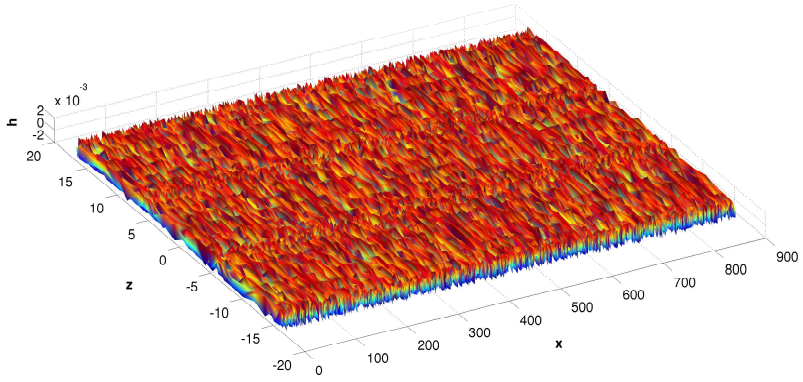

Figure 2.3: Random surface irregularities distribution over the flat plate.

2.2.4 A simple model for the natural surface roughness

A roughness element with the shape obtained according to

$$h(x,z) = \varepsilon_h h_x(x) \sum_{i=1}^{6} (sin(i\beta_0 z + \phi_{R,i})), \tag{2.13}$$

.

is applied to excite steady multi wavenumber crossflow instabilities with ϕ_R as a phase shift which is randomly chosen. As a result, the wavenumber of the spanwise modes are $k\beta_0$ in which i is $1, 2, ..., 6$. $h(x)$ is the same as the one defined in § 2.2.1 with the same parameters. β_0 is the fundamental mode specified by the width of the box. Also, ε_h is 0.0032.

Instead of prescribing the roughness element as a surface deformation, it is modeled in terms of inhomogeneous boundary conditions for the enforced disturbances. The same boundary condition as § 2.2.1 according to (2.11) is applied at the wall. It should be mentioned that here the Taylor series expansion used for specifying the non-homogeneous boundary conditions is truncated at first order.

2.3 Localised surface roughness as a control mechanism

In this section, a roughness element with the same shape as § 2.2.1 but with a different spanwise wavenumber is considered. The aim is to control excited

multiple spanwise instabilities initiated by the *natural* roughness studied in section 2.2.4. The latter is obtained by means of nonlinear interactions of the most amplified, *i.e. target*, and *control* modes.

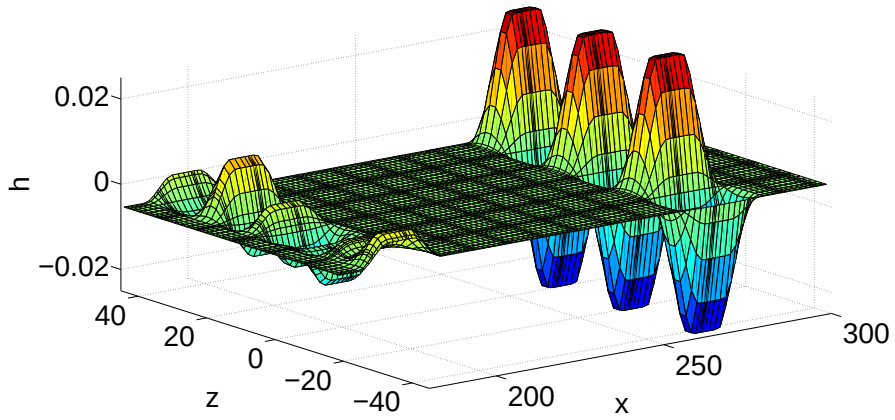

Figure 2.4: *Natural* and *control* roughness elements shapes in the physical space. The height of the *control* roughness is scaled by a factor of 0.1.

As the most unstable stationary crossflow mode in the FSC boundary layers has the spanwise wavenumber $\beta = 0.2$, the *target* mode is supposed to have the same spanwise wavenumber in the current studies. According to the experiments done by Saric *et al.* (1998), the spanwise wavenumber of the control mode should be 2/3 of the most unstable mode. As a result, the spanwise wavenumbers of the fundamental and *control* modes are $\beta_0 = 0.1$ and $3\beta_0 = 0.3$, respectively. Accordingly, the width of the computational box which obtained from $2\pi/\beta_0$ is equal to 62.8.

Table 2.1: *Natural* and *control* surface roughness parameters in (2.8), (2.10) and (2.13) for the roughness elements combination.

Roughness	ε_h	h_{start}	h_{end}	h_{rise}	h_{fall}
Natural	0.0032	11.6	32.2	11.5	11.5
$c1$	0.21	100	127.6	11.5	11.5
$c2$	0.32				

The shape of the combination of the *natural* and *control* surface roughness is represented in figure 2.4. Two different *control* roughness heights are studied to investigate the effect of increasing control surface roughness height to suppress

the target mode disturbance amplitudes. In current studies, $c1$ and $c2$ stands for *control* roughness with ε_h equal to 0.21 and 0.32, respectively. The inflow Reynolds number is fixed to 220. The other required parameters for the *natural* and *control* roughness elements are represented in Table 2.1.

Chapter 3

Numerical Method

The present simulations were carried out using the spectral element method (SEM) by Petra (1984). Patera solved the three-dimensional time-dependent Navier-Stokes equations which provides spectral accuracy in space along with geometrical flexibility and consequently applicable to complex geometries. The simulation code Nek5000 has been used here, was developed by Fischer *et al.* (2008).

3.1 Implementation

The computational domain is decomposed into a series of elements, which in turn are subdivided into arrays of Gauss-Lobatto-Legendre (GLL) nodes for the velocity field and Gauss-Lobatto (GL) nodes for the pressure field, respectively. The solution to the Navier-Stokes equations is approximated locally as a sum of orthogonal basis functions, *i.e.* Legendre polynomials, up to degree N. Complete details about the expansion of the flow variables ,the time integration scheme, and the spatial discritization are clearly described in Schrader *et al.* (2010). Here, $N = 9$ is selected for the velocity (GLL) grids and $N = 7$ for the pressure (GL) grids. This setup is based on $\mathbf{P}_N - \mathbf{P}_{N-2}$ discritization by Maday & Patera (1989) which means that the pressure grid is of order $N - 2$, staggered with respect to velocity grid.

3.2 Geometry, mesh, and boundary conditions

The geometry of the problem consists of different roughness shapes which are inserted into a rectangular box. The surface roughness is inserted by displacing the GLL nodes at the wall. Table 3.1 gives the dimensions L_x, L_y and L_z of the computational domain and the corresponding number of elements N_x, N_y and N_z along the spatial coordinate. The inflow Reynolds number for all cases is equal to 220. Two different computational boxes, A and B have been used to obtain the results for receptivity to different roughness elements defined in the

previous chapter.

Table 3.1: Dimensions and resolutions of the computational domain regards to the disturbance forcing types.

Box	$L_x \times L_y \times L_z$	$N_x \times N_y \times N_z$	Disturbances
A	$883.2 \times 20.0 \times 33.0$	$127 \times 9 \times 3$	§ 2.2.1 and §2.2.3
B	$3060.0 \times 41.667 \times 62.8$	$300 \times 15 \times 6$	§ 2.2.4 and § 2.3

The computational grid and GLL nodes for both distributed and natural surface roughness are shown in figure 3.1 for box A.

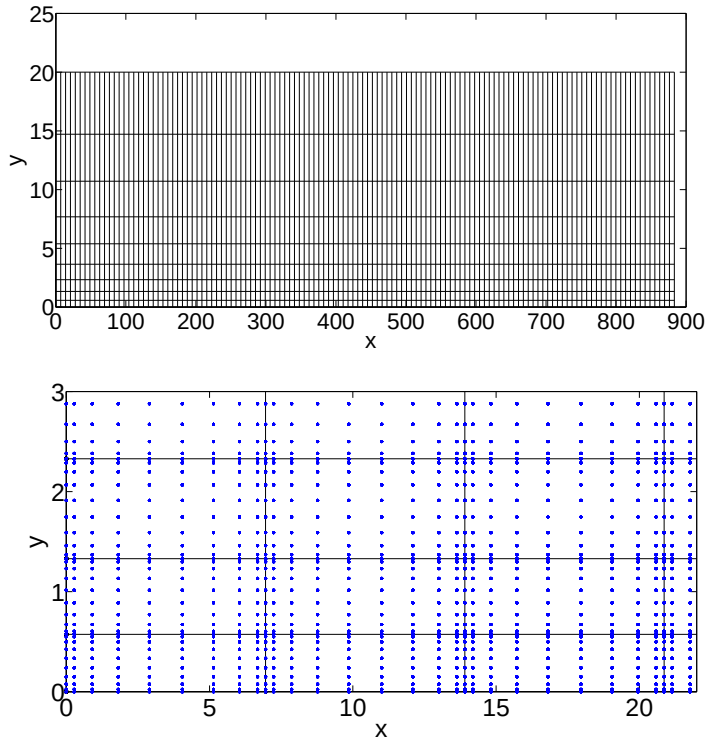

Figure 3.1: Computational grids and the GLL nodes for the simulations of the distributed-modeled and random roughness. Up: Spectral element mesh. Down: Showing the GLL nodes.

3.3 Performance of Nek5000

In this section, we present the performance of Nek5000 for the configuration studied here. We compare three criteria to qualify the parallel efficiency. As one can see in the Figure 3.2, the average speedup experiences the maximum for 256 processors compared to the linear speedup. Although 512 processors could be a good choice as well, these number of processors may not provide perfect quantity time. Therefore, we chose 256 processors for the current studies.[1]

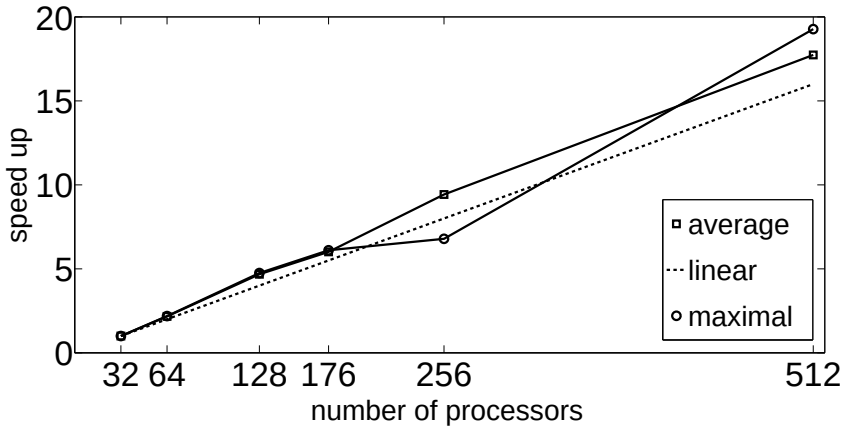

Figure 3.2: Speedups of Nek5000 by varying number of processors.

[1]Compute time was provided by National Super Computer (NSC) in Linköping, Sweden.

Chapter 4

Results and conclusions

The main goal of this work is to compare the different approaches of roughness modelling and study the stabilisation of the boundary layer by localised surface roughness. The current results are divided into four parts. First, the effect of a chordwise localized, spanwise periodic roughness element with different amplitudes on the receptivity is investigated. The roughness elements are meshed as well as modeled by applying non-homogeneous boundary conditions. The receptivity results obtained from both approaches will be compared. Furthermore, the boundary-layer receptivity to a random distributed surface irregularities is studied. In the end, the boundary layer is excited by a simple model of natural roughness. The dominant stationary crossflow mode initiated by the *natural* roughness is then controlled by a localised roughness downstream of the *natural* one.

4.1 Boundary layer receptivity to chordwise localized, spanwise periodic surface roughness

As noted earlier, the receptivity coefficient C_R is a criterion that represents the efficiency of the forcing mechanism to excite the least stable eigenmode among different modes excited inside the boundary layer. C_R is proportional to the receptivity amplitude A_R. Here, the response of the boundary layer is specified by the wall-normal maximum of $\sqrt{\overline{u^2}}$, where u is the chordwise disturbance velocity.

In this section, the boundary-layer response due to existence of the meshed surface bump of different wavenumber β_R is studied and displayed in figure 4.1. In each case, another DNS simulation of the evolution of the steady crossflow wave is performed. The boundary layer response to these initial conditions are shown as thin lines in the figure.

According to the figure, the flow response in the nearby region of the bump

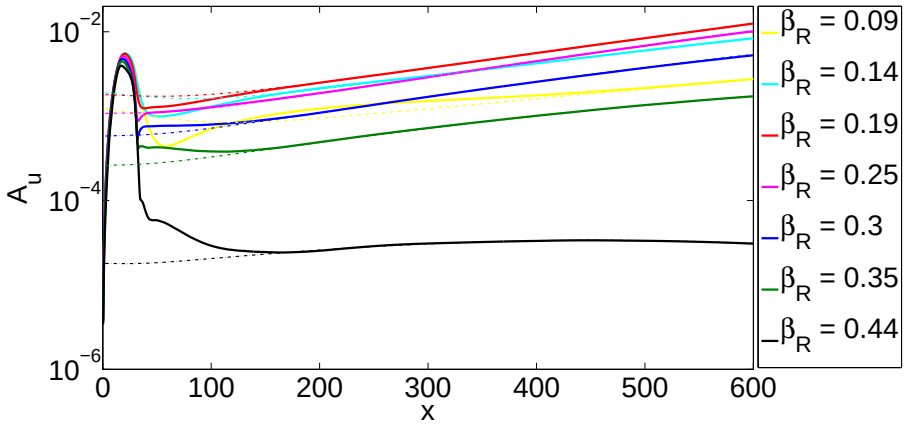

Figure 4.1: Boundary layer response to perturbations caused by the meshed surface bump at $x_R = 18.4$ (thick line), and the corresponding clean crossflow modes as obtained from a homogeneous solution (thin line) for different spanwise wavenumbers.

is characterised by transient behaviour, while the downstream evolution of the boundary layer disturbance is fully dominated by the excited stationary crossflow instability. Also, one can see in the figure that the receptivity efficiency is highly dependent on the spanwise wavenumber of the surface bump. The highest boundary layer receptivity is obtained for $\beta = 0.19$ among all other spanwise wavenumbers.

The chordwise roughness contour in Fourier space is shown in figure 4.2. $H(\alpha_{CF})$ shows to which degree the chordwise wavenumber of the triggered stationary crossflow mode is represented in the spectral shape function.

Figure 4.3 reveals that the surface roughness with short spanwise wavenumbers, resulting in the instabilities with large wavelengths, give higher receptivity coefficients. Among all β_R, the highest C_R is obtained for 0.14. Moreover, the dash line is the region in which the receptivity coefficient goes to infinity and decreases afterwards in a way that it reaches to different finite values, 0.0038 and $2.5993.10^{-4}$ for $\beta_R = 0.44$ in meshed and modeled cases, respectively. Comparison of the roughness shape in Fourier space with figure 4.3 represents that the jump occurs for α_{CF} and β_R around 0.4 and 0.41, respectively. A_R is small for $\beta_R = 0.44$ according to figure 4.1 and $H(\alpha_{CF}) \to 0$ for $\alpha_{CF} = 0.4$. As a result, the receptivity coefficient C_R is no longer well-defined as both numerator and denominator according to (2.12) become small.

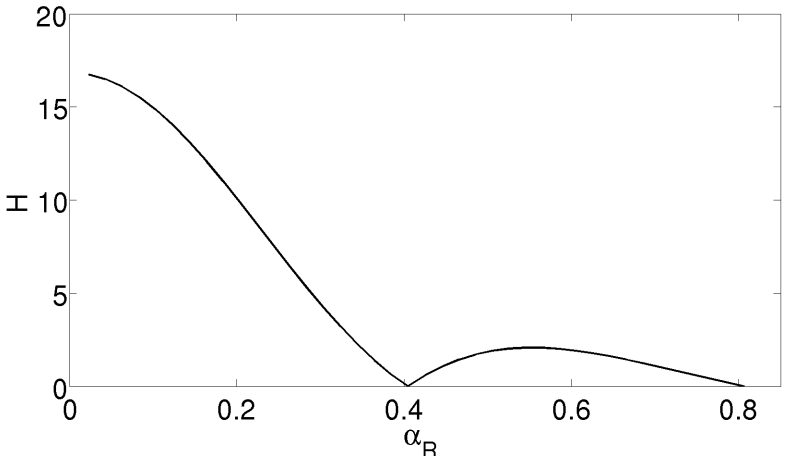

Figure 4.2: The roughness shape in spectral space.

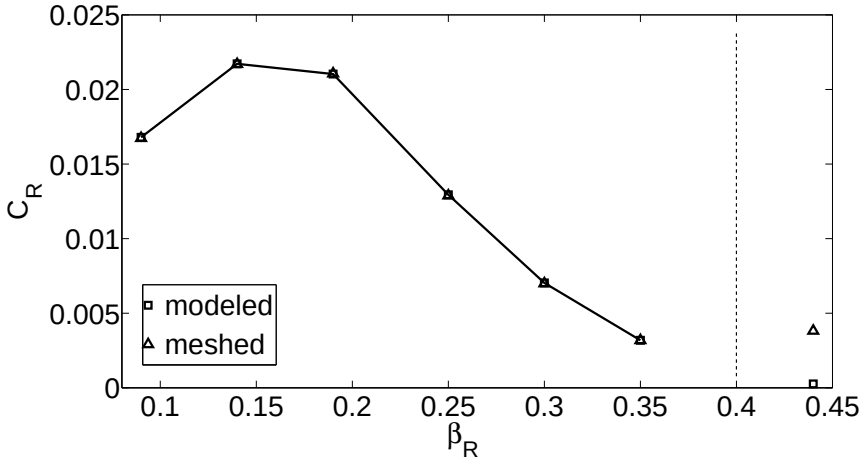

Figure 4.3: The effect of the spanwise wavenumber on the boundary layer receptivity to the surface bump (Thick line). The dashed line refers to the region of infinity value for C_R.

4.1.1 Meshed and modelled surface roughness

As mentioned in § 2.2.1, the roughness element is modeled by applying inhomogeneous boundary conditions and also considered as a surface deformation by inserting the bump into the numerical mesh. Figure 4.4 shows the boundary-layer response obtained by employing both approaches.

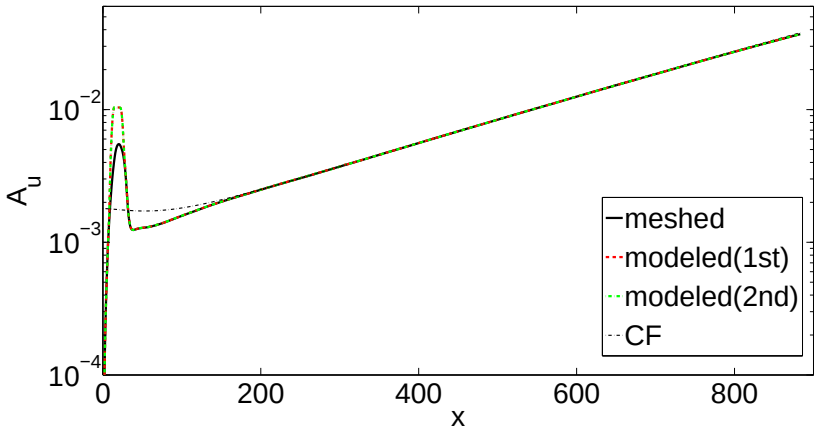

Figure 4.4: Boundary layer response to perturbations caused by meshed (black line), and modeled roughness element truncated to the first (red line) and second (green line) orders.

According to the figure, the response of the boundary layer downstream of the surface bump is independent of the way that the roughness element is implemented while there is a clear difference in the boundary-layer receptivity between the meshed and modeled cases in the vicinity of the surface roughness. Moreover, truncation of the Taylor series expansion defined in (2.11) to the first order works perfectly accurate for this bump height and the corresponding boundary-layer response overlaps the second order one.

4.1.2 The effect of roughness height

In the previous section, the boundary layer receptivity to the surface roughness with a specific amplitude and the receptivity coefficient C_R for different β_R were discussed. A_R, the amplitude of the excited unstable crossflow mode is proportional to ε_h, i.e. the maximum height of the surface bump. In this section, the influence of the surface roughness height on the boundary layer receptivity is studied in order to understand in which roughness amplitude the nonlinear behaviour begins to influence the receptivity. The $\varepsilon_{original}$ is the one investigated in the previous section and set to 0.021. The roughness elements with different amplitudes are both meshed and modeled (first and second order) and the receptivity results are compared.

The spanwise wave number β_R is set to 0.19 and the bump has the shape defined in § 2.2.1, but with different bump heights in the range of $0.04 \leq \varepsilon_h \leq 0.4$ which corresponds to 3.8% to 38% of the displacement thickness. Figure 4.5 shows the effect of the bump height on receptivity to roughness element. The figure

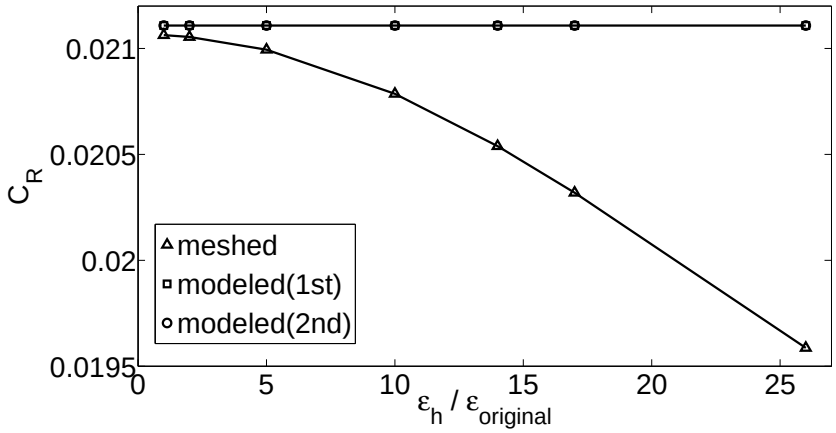

Figure 4.5: Bump height influence on the receptivity coefficient for the meshed (△) and first and second order modeled (□) surface roughness. $\varepsilon_{original} = 0.021$.

reveals that there is a region of linear growth of the unstable mode which is no longer identified for the highest roughness element amplitude. The nonlinear behaviour exists at even lower bump amplitude and the receptivity coefficient C_R clearly becomes dependent on the surface roughness height beyond $\varepsilon_h = 0.05$.

The figure reveals that truncation of Taylor series expansion to the first order gives the same receptivity results as expanding it up to the second order for all the bump heights studied here.

Figure 4.6 shows the disturbances amplitudes for different heights of the roughness elements. It is clear that the disturbances amplitudes for the modeled case perfectly match the meshed one until the surface roughness height increases to 20% of the dispalcement thickness. This value corresponds to the roughness height equal to the original bump amplitude multiplied by a factor of 10. The disturbances amplitude difference for the meshed surface roughness reaches 93% of the disturbance amplitude of the modeled bump for the highest roughness element amplitude.

4.2 Boundary layer response to random distributed surface roughness

The response of the boundary layer to the random distributed surface irregularities is shown in the figure 4.7 for fundamental mode, first, and second harmonics, respectively.

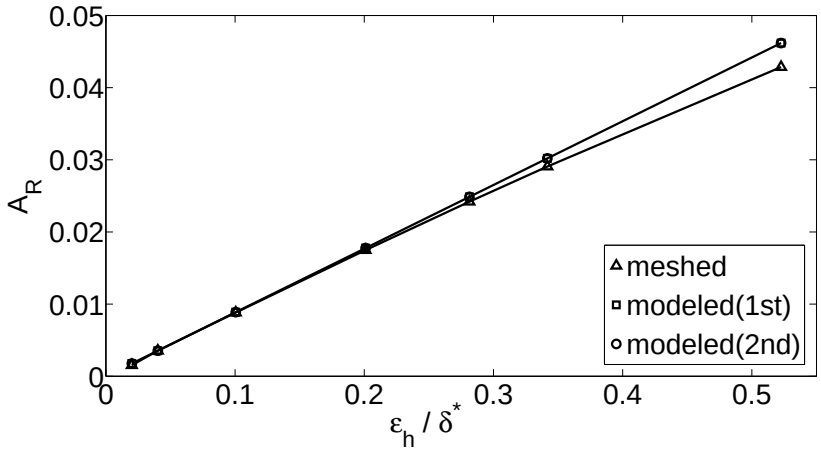

Figure 4.6: Surface roughness height effect on the disturbance amplitudes for the meshed and modeled cases. The (□) refers to both first and second modeled bump.

The non-linear interaction of the disturbances modes results in different receptivity amplitudes for the linear and non-linear simulations. The non-linear results show less disturbances amplitude of the fundamental mode compared to the linear case while the first harmonic amplified more for the nonlinear one. Due to the small height of the random distributed surface roughness, the second harmonic shows not that much difference in the disturbances amplitudes for two cases.

4.3 Boundary layer response to natural roughness element

In this section, we investigate the three-dimensional boundary layer receptivity to natural roughness with the shape defined in section 2.2.4. In figure 4.8 it can be observed that all the modes are strongly amplified first and the modes β_0, $2\beta_0$, $3\beta_0$ and $4\beta_0$ are growing throughout the whole domain.

Although the mode β_0 is detected, $2\beta_0$ contains the most contribution of the disturbances energy over the entire plate. This mode amplifies exponentionally immediately after the roughness location, experiences a permanent disturbances growth and then saturates. Also, it is interesting that mode $4\beta_0$ grows rapidly for $1000 \leq x \leq 2500$ and begins to saturate afterward.

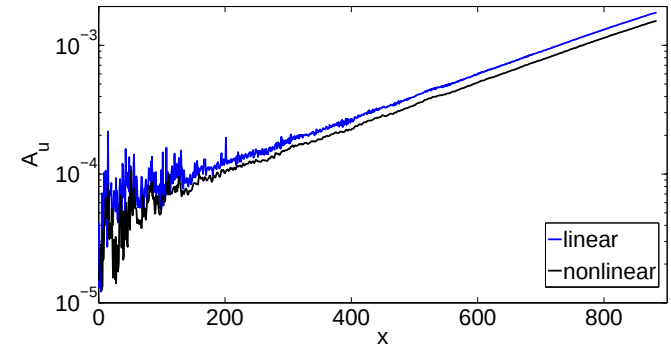

(a)

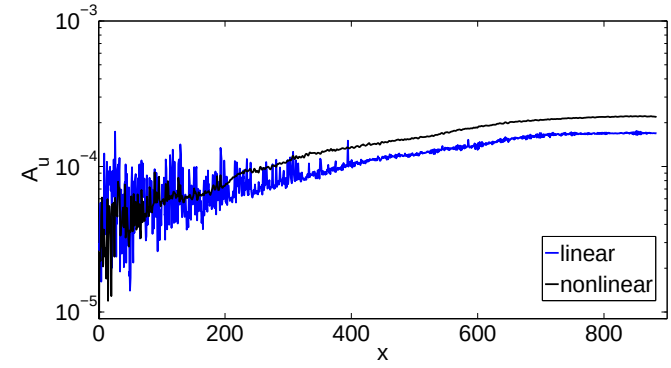

(b)

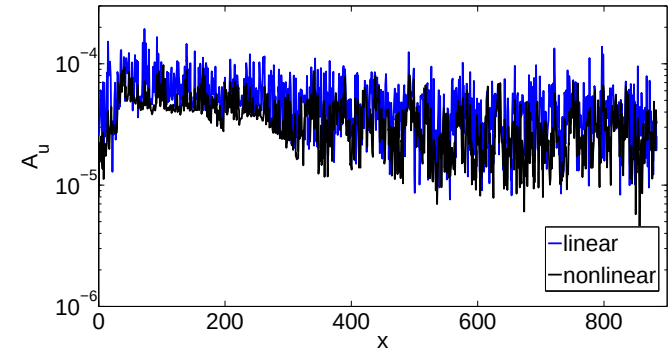

(c)

Figure 4.7: Boundary layer response to perturbations caused by natural surface irregularities for linear (black line) and non-linear (blue line) cases of (a) the fundamental mode, (b) first harmonic, and (c) second harmonic.

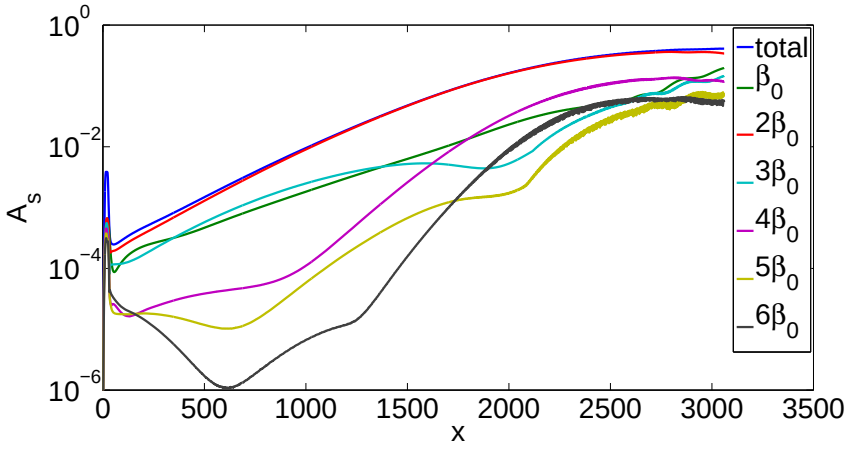

Figure 4.8: Response of the boundary layer to the distributed surface irregularities with $\varepsilon_h = 0.0032$.

4.4 Disturbances control by surface roughness

In the previous section, the *natural* roughness was localized to initiate multiple steady disturbances. The results show that mode $2\beta_0$ *i.e. target* mode becomes dominant. In this section, two sets of roughness elements with different heights are applied downstream of the *natural* roughness to suppress the target mode amplitude initiated by the surface bump defined in §(4.3). These two sets of, the so called *control* roughness elements, are defined according to (2.8) and (2.10) with $h_{start} = 100$ and $h_{end} = 127.6$.

According to the experimental results obtained by Saric *et.al* (1998) and Wassermann and Kloker (2002), the control roughness element should be arranged such that the wavelength of the surface bump is less that the wavelength of the most unstable mode. The authors found that applying a control roughness element with a sub-critical spacing equal to 2/3 of the wavelength of the most unstable mode results in transition delay of a swept-wing boundary layer beyond the pressure minimum and toward the trailing-edge. As a consequence, the spanwise wavenumber β_R of the control mode in the current studies is chosen as 0.3. This mode is forced and disturbances amplitude reduction should be observed in the target mode.

The boundary layer response to the surface bump in the existence of the control roughness elements with different heights are presented in the following. Moreover, the results are compared to the case without imposing the control mechanism. As noted before, the control roughness elements with ε_h equal to 0.21 and 0.32 are named $c1$ and $c2$, respectively.

4.4.1 Stabilisation of the boundary layer

As mentioned earlier, periodic surface roughness with spanwise wavenumber equal to the wavenumber of the second harmonic mode of the disturbances discussed in §(4.3) are applied to stabilise the target mode (first harmonic here) and reduce the disturbances amplification. Two different values of ε_h equal to 0.21 and 0.32 for the control roughness height are studied.

The wavy structures whiche sounds to be "roll over "is observed in figure 4.9. The latter shows the existence of steady cross flow instabilities. The dominance of a single cross flow mode is appreant upstream since the wavy structures are fairly even and regular there while the competition of different modes results in an irregular structure downstream,.

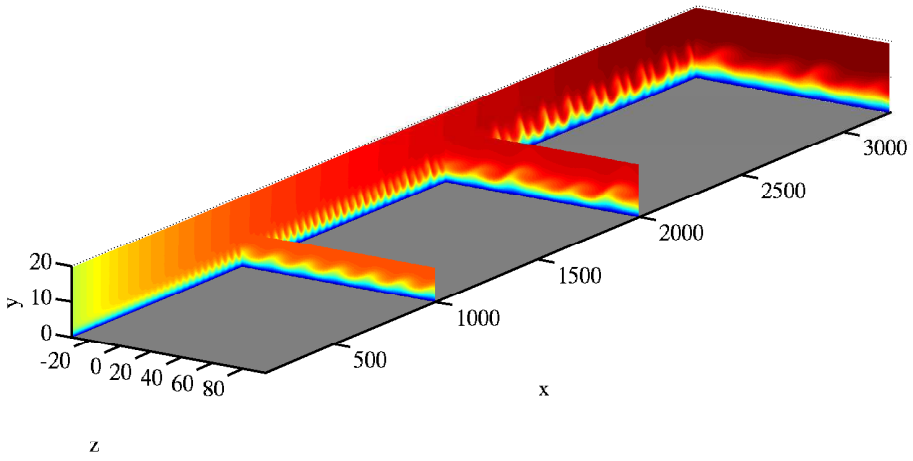

Figure 4.9: Total velocity component $(U + u')$ for the control case with $\varepsilon_h = 0.32$.

Figure 4.10 reveals that the *target* mode is excited at the surface roughness and grows rapidly afterwards for both cases. This mode then saturates at $x = 2500$ for $c1$ while a strong disturbances amplitude reduction is observed for $c2$. The mode β_0 experiences the same trend as the target mode but with a smaller disturbances amplitude up to $x = 2500$. This a location at which the mode β_0 starts to amplify for $c1$ and a sharp reduction for $c2$.

The most amplified mode in the vicinity of the surface bumps for both cases appears nearby the higher amplitude control roughness. This disturbance amplification corresponds to the mode β_0, i.e. *control* mode, which contains the most energy contribution in that region. This mode reaches a maximum at $x = 1400$, experiences a slight decay and then starts to amplify a bit at $x = 2500$ for $c1$ while the other case shows a graduate reduction after $x = 2500$. Total distur-

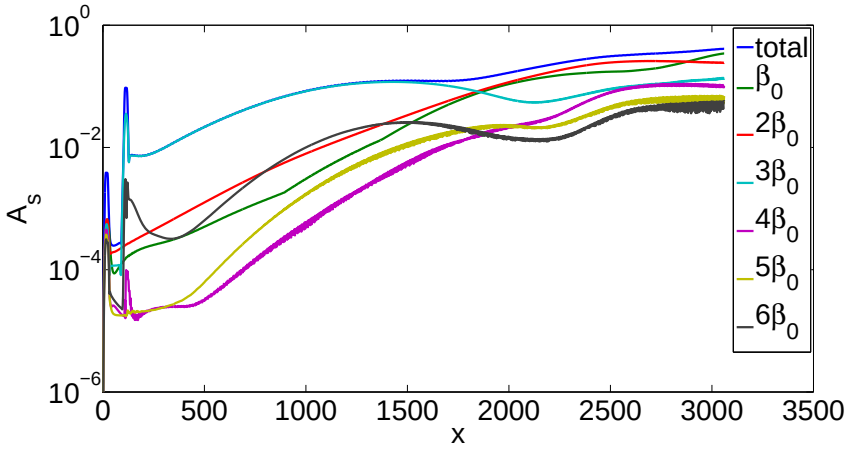

(a) c1

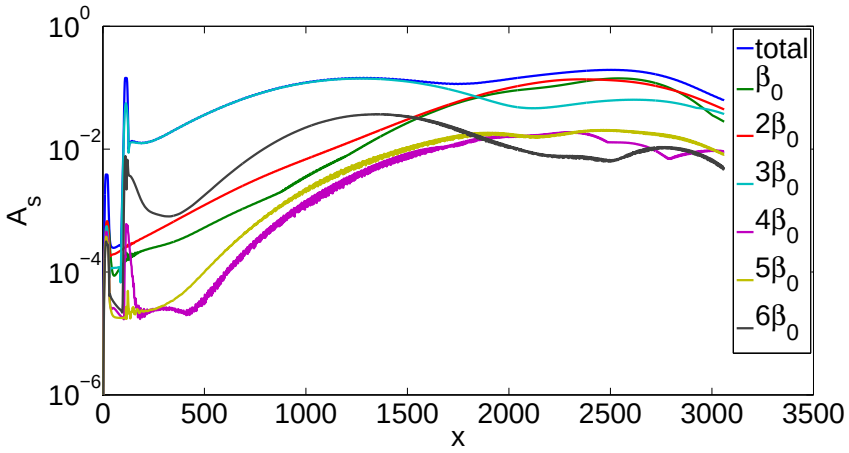

(b) c2

Figure 4.10: Boundary layer receptivity to the distributed surface irregularities with control surface roughness. (a) $c1$. (b) $c2$.

bances modes for both control cases experience the same trend as the *control* mode until $x = 1500$ with higher disturbances amplitude at the position of roughness elements. Afterwards, the behaviour of this mode is similar to the *target* mode.

One can see in the figure that the second most amplified disturbances mode in the region of the bumps for both control surface roughness heights is allocated to the mode $6\beta_0$ due to nonlinear interaction. Furthermore, although the control roughness element is made of a single spanwise wavenumber, the super-

harmonic modes are forced in the vicinity of the surface roughness as a result of non-linear interactions.

4.4.2 Comparison of the receptivity results with and without control

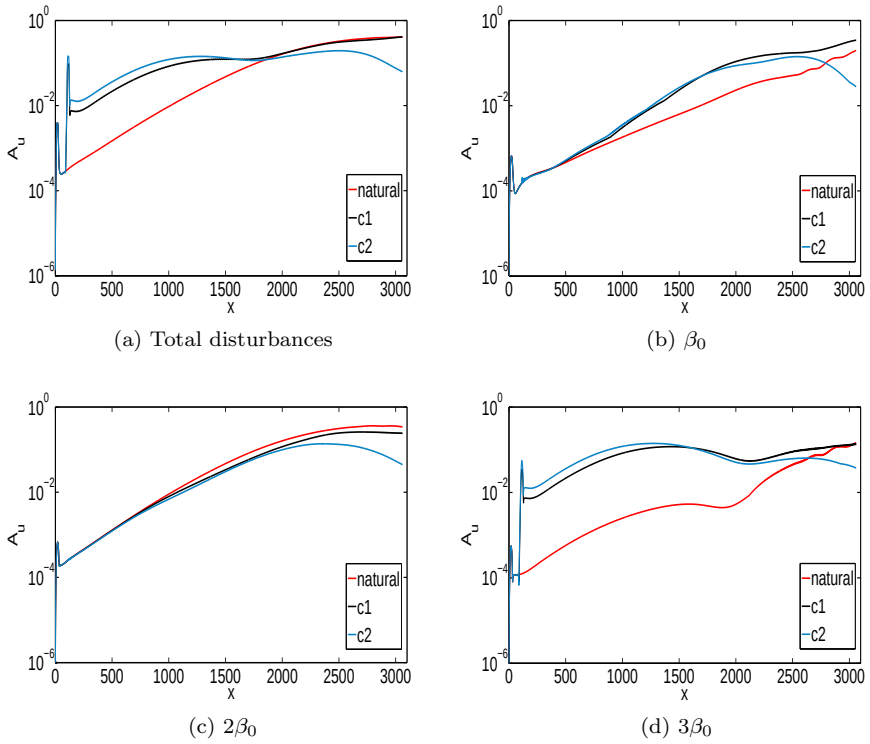

(a) Total disturbances

(b) β_0

(c) $2\beta_0$

(d) $3\beta_0$

Figure 4.11: Comparison of the boundary layer respones in the presence of surface roughness of natural and control cases. (a) Total disturbances. (b) Fundamental mode. (c) *Target* mode. (d) *Control* mode.

In order to a better understanding of the role of the control roughness with respect to damping the disturbances and a possible transition delay, the results obtained in sections 4.3 and 4.4.1 are plotted here. Comparing the results shows that the *target* mode still has the most energy contribution downstream of the surface irregularities among other modes in the control cases. It can be observed in the figure 4.11(a) that the total disturbances for the control case $c2$ attain the largest disturbances amplitude until $x = 1500$, thereafter the other control case catch the highest total disturbances amplitude. $x = 2000$ is the position after which $c2$ has the lowest total disturbances energy. Further, the *control* modes of $c1$ and $c2$ behaves as the total disturbances amplitude.

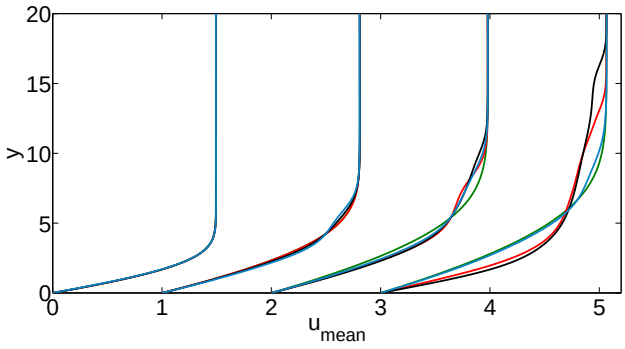

(a)

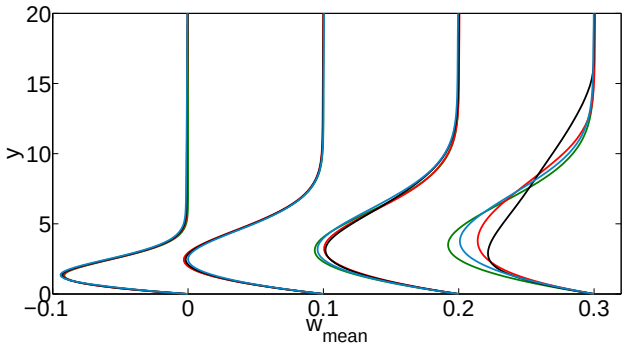

(b)

Figure 4.12: (a) Stream- and (b) spanwise base and distorted mean (bf + $(0,0)$ mode) flow profiles at various downstream positions (x = 112.2, 1132.2, 2264.8 and 3060 from left to right). The abscissa shift is 1 and 0.1 for the stream- and spanwise directions, respectively. The green line is for the undisturbed base flow and the red, black and blue lines are allocated to the distorted mean flow of the *natural* roughness and controlled cases $c1$ and $c2$, respectively.

According to figure 4.11(b), $c1$ has the largest amplitude of the fundamental mode over the whole domain. A comparison of the boundary-layer response with and without applying control roughness in the figure 4.11 shows clear differences in the disturbances amplitudes. Moreover, it is apparent that increasing the amplitude of the control mode results in a reduction in the target mode amplitude.

The undisturbed base flow (bf) and the distorted mean (bf+$(0,0)$ mode) flow at different downstream positions are shown in figure 4.12 for the chord- and spanwise directions. The mean flow distortions as a result of the nonlinear interactions of the crossflow modes are evident in the figure. Both velocity profiles

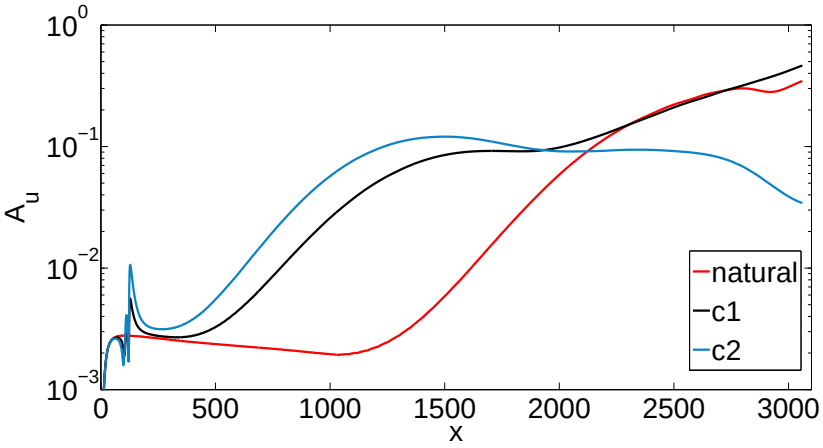

Figure 4.13: The base flow distortion of the natural roughness and control cases.

get fuller close to the wall downstream. Furthermore, the crossflow disturbances are stabilised due to the crossflow reduction as a result of the mean-flow distortion. The figure reveals that the mean flow of $c2$ distorts the most upstream of the flow while the maximum distortion is allocated to $c1$ downstream. These results are reffered to Wassermann and Kloker (2002) who applied upstream flow distortion (UFD) technique to stabilise the most dangerous mode by means of applying a spanwise row of roughness elements near the leading edge.

The base flow distortion of the disturbed cases are presented in figure 4.13. The corresponding disturbances amplitudes are almost the same until $x = 100$ after which the uncontrol case shows a slight decay till $x = 1200$ and starts to grow rapidly afterwards. The control case with $c2$ show fluctuations in a small region, strongly amplify and attain the maximums at $x = 1400$; thereafter it decays and at the outflow the amplitude is 28% of the maximum amplitude. The other control case shows the same trend until $x = 1400$, although it has lower disturbances amplitude of the base flow distortion. Afterwards, the growth is almost weakened but still has the highest disturbances amplitudes among all cases except between $2300 \leq x \leq 2700$ in which the uncontrol mode contains a rather higher amplitude.

Chapter 5

Conclusions

In this thesis we perform direct numerical simulations to study the receptivity and stabilisation of a three-dimensional boundary-layer on a swept flat plate. A direct receptivity mechanism, chordwise localised, spanwise periodic surface roughness is applied to excite the boundary layer. The base flow is the solution of the Navier-Stokes equations with Falkner-Skan-Cooke velocity profiles as the initial condition. The sweep angle is 45° and the Hartree parameter corresponds to the free-stream acceleration is set to 0.3.

Two different approaches are used to model the roughness elements. The surface bumps are inserted into the numerical mesh as well as modeled by applying inhomogeneous boundary conditions along the wall. The present results show that the boundary layer response downstream of the surface roughness is the same for both two approaches for different roughness spanwise wavenumbers β_R except $\beta_R = 0.44$.

The effect of roughness height on the boundary-layer receptivity for a specific $\beta_R = 0.19$, the most receptive spanwise wavenumber is investigated. The results reveal that the receptivity coefficient C_R is dependent on the roughness height ε_h beyond 0.05 where the nonlinear behaviour appears. Also, A_R for the modeled surface roughness perfectly matched the meshed one for the roughness height below 20% of the displacement thickness.

A simple model for natural surface roughness is implemented by applying modeled roughness approach. The nonlinear saturation of the linearly most unstable, *i.e target* mode as a result of excitation of crossflow disturbances is observed. The latter is stabilised by means of using *control* roughness downstream of the *natural* one. The *control* roughness has the wavenumber 2/3 of the target mode in accordance with the experiment by Saric *et al.* (1998). The nonlinear mode interactions suppress the *target* mode. In agreement with the numerical studies of Wassermann and Kloker (2002), this nonlinear effect results in meanflow modification which leads to stabilise the most unstable crossflow modes. Moreover,

the results show that increasing the amplitude of the control mode suppress the *target* mode the most.

As possible extensions, one may consider the secondary, non-stationary instabilities. Similar work was performed by Tempelmann *et al.* (2011) where they applied localised surface roughness in order to stabilise a swept-wing boundary layer by means of direct numerical simulations. The results show that control surface roughness is an effective mechanism to suppress transition excited by both steady and unsteady disturbances.

Bibliography

[1] L.U. Schrader, L. Brandt, D.S. Henningson, 2009b, Receptivity mechanisms in three-dimensional boundary-layer flows. J. Fluid Mech., vol. 618, 209-241.

[2] W.S. Saric, H.L. Reed, E.B. White, 2003, Stability and transition of three dimensional boundary layers. Annu. Rev. Fluid. Mech., vol. 35, 413-40.

[3] M.S. Reibert, W.S. Saric, R.B. Jr. Carillo, K.L. Chapman, 1996, Experiments in nonlinear saturation of stationary crossflow vortices in a swept-wing boundary layer. AIAA Paper96-0184.

[4] P.J. Schmid, D.S. Henningson, 2000, Stability and transition in shear flows. vol. 142. ISBN 0-387-98985-4.

[5] D. Tempelmann, A. Hanifi, D.S. Henningson, 2010, Spatial optimal growth in three-dimensional boundary layers. J. Fluid Mech., vol. 646, 5-37.

[6] P. Wassermann, M. Kloker, 2002, Mechanisms and passive control of crossflow-vortex-induced transition in a three-dimensional boundary layer. J. Fluid Mech., vol. 456, 49-84.

[7] S. Bake, A.V. Ivanov, H.H. Fernholz, K. Neemann, Y.S. Kachanov, 2002, Receptivity of boundary layers to three-dimensional disturbances. Eur.J. Mech.B/Fluids , vol. 21, 29-48.

[8] A.A. Maslov, A.N. Shiplyuk, A.A. Sidorenko, D. Arnal, 2001, Leading edge receptivity of a hypersonic boundary layer on a flat plate. J. Fluid Mech., vol. 426, 73-94.

[9] O.M. Haddad, T.C. Corke, 1998, Boundary layer receptivity to free-stream sound on parabolic bodies. J. Fluid Mech., vol. 368, 1-26.

[10] V.R. Gaponenko, A.V. Ivanov, Y.S. Kachanov, J.D. Crouch, 2002, Swept-wing boundary-layer receptivity to surface non-uniformities. J. Fluid Mech., vol. 461, 93-126.

[11] S.S. Collis, S.K. Lele, 1999, Receptivity to surface roughness near a swept leading edge. J. Fluid Mech., vol. 380, 141-168.

[12] W.S. Saric, H.L. Reed, E.J. Kerschen, 2002, Boundary-layer receptivity to freestream disturbances. Annu. Rev. Fluid. Mech., vol. 34, 291-319.

[13] F.P. Bertolotti, 2002, Receptivity of three-dimensional boundary-layers to localized wall roughness and suction. Phys. Fluids, vol. 12, 1799-809.

[14] R.H. Jr. Radeztsky, M.S. Reibert, W.S. Saric, 1999, Effect of isolated micron-sized roughness on transition in swept-wing flows. AIAA J., vol. 37, 1371-77.

[15] M. Choudhari, 1994, Roughness-induced generation of crossflow vortices in three-dimensional boundary layers. Theoret. Comput. Fluid Dynamics, vol. 6, 1-30.

[16] J.D. Crouch, 1993, Receptivity of three-dimensional boundary layers. AIAA Paper 93-0074.

[17] W.S. Saric, R.B. Jr. Carillo, M.S. Reibert, 1998, Leading-edge roughness as a control mechanism. AIAA Paper 98-0781.

[18] M. Choudhari, C.L. Chang, C. Streett, M. Carpenter, 2009, Roughness based crossflow transition control : A computational assessment. AIAA-2009-4105.

[19] H. Bippes, 1997, Environmental conditions and transition prediction in 3-D boundary layers. AIAA Paper 97-1906

[20] H. Bippes, 1999, Basic experiments on transition in three-dimensional boundary layers dominated by crossflow instability. Prog. Aerosp. Sci. 35, 363-412